

# Can Two-Dimensional IR-ECD Mass Spectrometry Improve Peptide de Novo Sequencing?

Maria A. van Agthoven,<sup>§</sup> Alice M. Lynch,<sup>§</sup> Tomos E. Morgan,<sup>§</sup> Christopher A. Wootton,<sup>§</sup> Yuko P.Y. Lam,<sup>§</sup> Lionel Chiron,<sup>†</sup> Mark P. Barrow,<sup>§</sup> Marc-André Delsuc,<sup>‡,+</sup> and Peter B. O'Connor<sup>\*,§</sup>

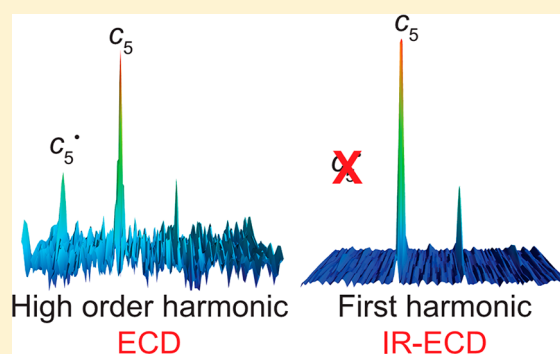
<sup>§</sup>Department of Chemistry, University of Warwick, Gibbet Hill Road, Coventry CV4 7AL, United Kingdom

<sup>†</sup>CASC4DE, Le Lodge, 20 av. du Neuhof, 67100 Strasbourg, France

<sup>‡</sup>Institut de Génétique et de Biologie Moléculaire et Cellulaire, INSERM, U596; CNRS, UMR7104, Université de Strasbourg, 1 rue Laurent Fries, 67404 Illkirch-Graffenstaden, France

## Supporting Information

**ABSTRACT:** Two-dimensional mass spectrometry (2D MS) correlates precursor and fragment ions without ion isolation in a Fourier transform ion cyclotron resonance mass spectrometer (FTICR MS) for tandem mass spectrometry. Infrared activated electron capture dissociation (IR-ECD), using a hollow cathode configuration, generally yields more information for peptide sequencing in tandem mass spectrometry than ECD (electron capture dissociation) alone. The effects of the fragmentation zone on the 2D mass spectrum are investigated as well as the structural information that can be derived from it. The enhanced structural information gathered from the 2D mass spectrum is discussed in terms of how de novo peptide sequencing can be performed with increased confidence. 2D IR-ECD MS is shown to sequence peptides, to distinguish between leucine and isoleucine residues through the production of  $w$  ions as well as between C-terminal ( $b/c$ ) and N-terminal ( $y/z$ ) fragments through the use of higher harmonics, and to assign and locate peptide modifications.



Two-dimensional mass spectrometry (2D MS)<sup>1</sup> is a method for tandem mass spectrometry that relies on correlation between precursor and fragment ions without ion isolation. 2D MS was first developed on a Fourier transform ion cyclotron resonance mass spectrometer (FTICR MS)<sup>2</sup> by Gäumann et al.<sup>3–5</sup> after an experiment in ion de-excitation by Marshall et al.<sup>6</sup> Although 2D MS was first developed in the late 1980s, the computational capacities necessary for data processing and data storage were insufficient to develop useful applications.<sup>1</sup> The theory of 2D MS was explored,<sup>7</sup> alternative methods such as Hadamard transformation methods<sup>8</sup> and stored waveform ion radius modulation<sup>9,10</sup> were developed, and the behavior of scintillation noise in 2D mass spectra was first analyzed.<sup>11</sup> In the early 2010s, 2D MS was revived and applied to commercial instruments with infrared multiphoton dissociation (IRMPD)<sup>12</sup> and electron capture dissociation (ECD)<sup>13</sup> as fragmentation methods. The pulse sequence for 2D MS was optimized,<sup>14</sup> denoising algorithms were developed for the removal of scintillation noise,<sup>15,16</sup> and user-friendly data processing and visualization software was developed.<sup>17</sup> 2D MS has been successfully applied to the analysis of small molecules,<sup>18</sup> polymers,<sup>19</sup> and both bottom-up<sup>20,21</sup> and top-down proteomics.<sup>22</sup> Recently, a method for 2D MS in a linear ion trap has been proposed.<sup>23</sup> Techniques to improve resolution in the vertical dimensions have also been investigated.<sup>24</sup>

Infrared activated electron capture dissociation (IR-ECD) is a subset of activated ion electron capture dissociation (AI-ECD), in which ions are activated by infrared irradiation<sup>25</sup> rather than collisional activation.<sup>26</sup> IR-ECD of peptides has been shown to increase fragmentation efficiency and cleavage coverage over ECD and is able to increase production of amino acid side-chain losses which can be used to differentiate some amino-acid residues, such as leucine and isoleucine.<sup>25</sup> Comparing ECD and IR-ECD MS/MS spectra has also shown that the two methods in combination can be used to differentiate N-terminus fragments from C-terminus fragments through the observation of  $c^*$  and  $z^*$  fragment abundances.<sup>27</sup> Developing a two-dimensional IR-ECD mass spectrometry (2D IR-ECD MS) can therefore be beneficial for the analysis of peptide mixtures, especially sequencing of unknown peptides.

De novo sequencing of a peptide is an important area of proteomics, pharmaceutical, and biomedical research.<sup>28</sup> MS/MS spectra of peptides are recorded and analyzed either by hand or with various algorithms in order to determine their amino acid sequence.<sup>29</sup> This study shows how 2D IR-ECD MS can be optimized and used to sequence peptides and

**Received:** December 20, 2017

**Accepted:** February 8, 2018

**Published:** February 8, 2018

distinguish isomeric residues with the examples of substance P and the tryptic digest of cytochrome *c*. This study also demonstrates that the zones for IR and ECD irradiation do not completely overlap in the ion cyclotron resonance (ICR) cell, which can be used to enhance the sequence information that is available in the 2D mass spectrum but that is not accessible by performing one-dimensional MS/MS. Finally, an easy method to identify and locate peptide modifications in 2D MS is also discussed.

## EXPERIMENTAL METHODS

**Sample Preparation.** Substance P and angiotensin I were purchased from Sigma-Aldrich (Dorset, United Kingdom) and used as received. Cytochrome *c* tryptic digest was purchased from Thermo Scientific (Amsterdam, The Netherlands) and dissolved in a stock solution of 95% purified water obtained from a Direct-Q3 Ultrapure Water System (Millipore, Nottingham, United Kingdom), 4.9% acetonitrile (VWR, Lutterworth, United Kingdom) with 0.1% formic acid (Sigma-Aldrich, Dorset, United Kingdom) at a concentration of 8 pmol/ $\mu$ L.

Substance P and angiotensin I were prepared in a solution of 75% water, 24.9% acetonitrile, and 0.1% formic acid at a concentration of 1 pmol/ $\mu$ L. The cytochrome *c* tryptic digest was prepared in a solution of 75% water, 24.9% acetonitrile, and 0.1% formic acid at a concentration of 800 fmol/ $\mu$ L.

**Instrument Setup.** All experiments were performed on a 12 T solariX Fourier transform ion cyclotron resonance mass spectrometer (Bruker Daltonik, GmbH, Bremen, Germany) with a nano-electrospray (nESI) ion source operated in the positive-ion mode with a 7–8  $\mu$ L/hour flow rate. Infrared ion activation was achieved using a Synrad 48–2 25 W CO<sub>2</sub> laser with a 10.6  $\mu$ m wavelength operated at 50% power (Mukilteo, WA, U.S.A.). Electron capture dissociation was achieved with an indirectly heated hollow cathode dispenser with a current set at 1.5 A.<sup>30</sup>

All one-dimensional mass spectra were recorded with 4Mword (16 bit) transients (1.6777 s). Mass ranges varied from  $m/z$  147.4–1500 to  $m/z$  147.4–3000, corresponding to frequency ranges from 1250 to 122.8 kHz to 1250–56.4 kHz. Pulse amplitudes were set at 15% excitation, i.e., 70  $V_{pp}$ , with 20  $\mu$ s per frequency and 625 Hz frequency decrements. Table S1 in the Supporting Information lists the instrument parameters used for each sample.

Scheme 1a shows the pulse sequence used to map fragmentation zones for each fragmentation method.<sup>14</sup> All pulses were broadband and cover the detected mass range (see

**Scheme 1. Pulse Sequence for (a) Fragmentation Zone Mapping and (b) Two-Dimensional IR-ECD Mass Spectrometry Experiment**

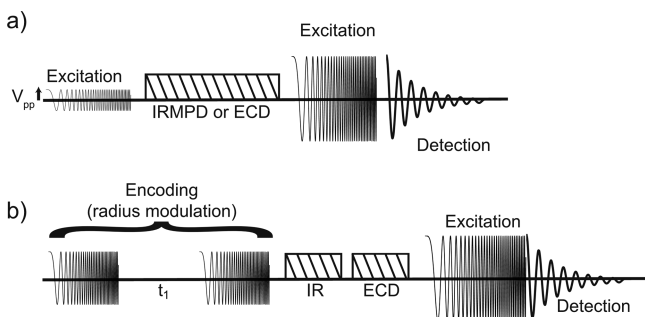


Table S1 in the Supporting Information). The first pulse amplitude ranged from 0 to 250  $V_{pp}$  with a pulse length of 2  $\mu$ s per frequency. The second pulse was the default excitation pulse (70  $V_{pp}$  and 20  $\mu$ s per frequency pulse length). The fragmentation parameters are listed in Table S1 of the Supporting Information.

Scheme 1b shows the pulse sequence for the 2D MS experiment. All pulses were broadband and covered the detected mass range (see Table S2 in the Supporting Information). The two first pulses were identical with 180  $V_{pp}$  amplitudes and pulse lengths of 1  $\mu$ s per frequency. The third pulse was the default excitation pulse (70  $V_{pp}$  and 20  $\mu$ s per frequency pulse length). The fragmentation parameters are listed in Table S1 of the Supporting Information. Incremental delays  $t_1$  are also listed in Table S2 of the Supporting Information, along with the corresponding Nyquist frequencies, vertical mass ranges, and horizontal mass ranges.

**Data Processing.** All one-dimensional mass spectra were first externally calibrated by the solariXcontrol software (Bruker Daltonics, Billerica, MA, U.S.A.) using Agilent ESI-L Low Concentration Tuning Mix (Agilent Technologies, Stockport, United Kingdom).<sup>31</sup> All the one-dimensional mass spectra were subsequently internally calibrated using a quadratic calibration equation in the Data Analysis 4.0 software (Bruker Daltonik, GmbH, Bremen, Germany).<sup>32,33</sup>

The MS/MS spectra acquired with the pulse sequence presented in Scheme 1a were processed and analyzed in 64-bit Python programming language on a commercial platform distributed by Anaconda Continuum Analytics (Austin, TX, U.S.A.) using modules and functions from the Spectrometry Processing Innovative Kernel (SPIKE) software.<sup>17</sup> An example of this program is shown in Figure S2 in the Supporting Information.

The data processing for 2D mass spectra has been explained in a previous article.<sup>21</sup> Both the data processing and the data visualization were performed using the SPIKE software.<sup>17</sup> The data processing was performed in a parallelized fashion on 128 processors of the High Performing Computer clusters at the University of Warwick and took 3.5 h. The urQRD denoising rank, when used, was set at 7.<sup>16</sup> Both external calibration and internal calibration using a quadratic frequency-to-mass conversion were applied.<sup>31–33</sup>

## RESULTS AND DISCUSSION

**Mapping the Fragmentation Zone for IR-ECD in the ICR cell.** Figure 1a shows the fragmentation efficiency for IRMPD and ECD as a function of the peak-to-peak amplitude of the first pulse in the pulse sequence shown in Scheme 1a, allowing mapping of the IRMPD and ECD fragmentation zones. Angiotensin I was chosen for IRMPD fragmentation zone mapping and substance P for ECD, because they fragment particularly well with these methods. Because ion cyclotron radii are proportional to the amplitude of the excitation pulse,<sup>34</sup> the pulse sequence shown in Scheme 1a enables the mapping of the fragmentation zone.<sup>14</sup> The fragmentation efficiency was defined as

$$F = \frac{\sum A_{\text{fragments}}}{A_{\text{precursor}} + \sum A_{\text{fragments}}} \quad (1)$$

in which  $F$  is the fragmentation efficiency,  $A_{\text{precursor}}$  is the signal intensity of the precursor ion, and  $A_{\text{fragment}}$  is the signal intensity of a fragment ion.

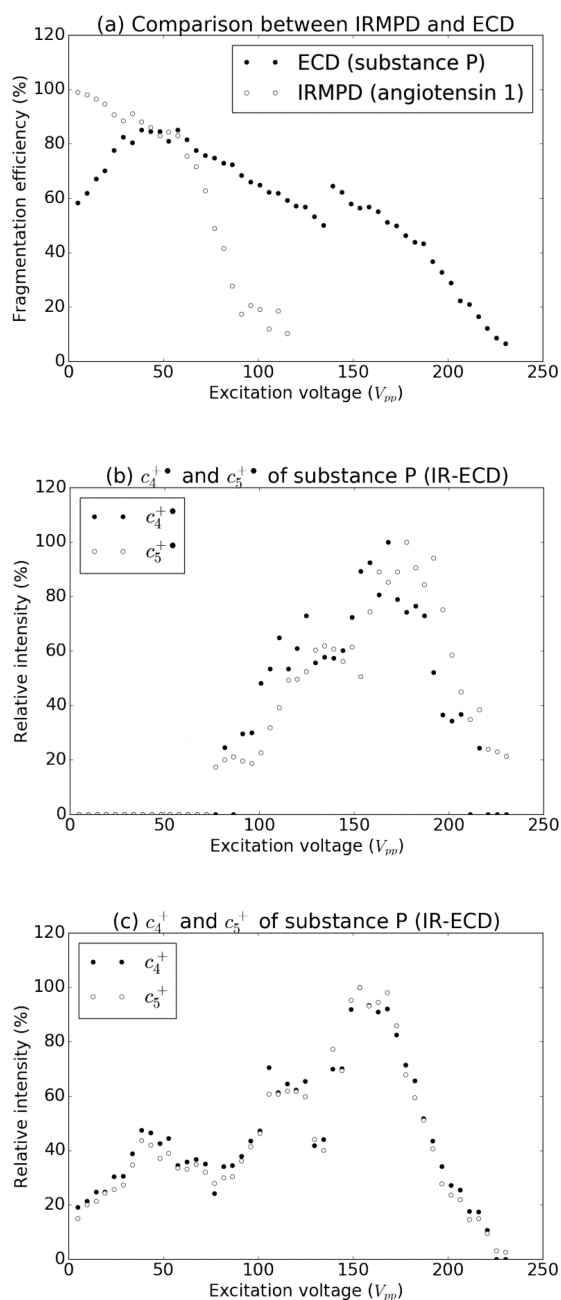


**Figure 1.** Fragmentation zone mapping with the pulse sequence in Scheme 1a. (a) Fragmentation efficiency vs excitation amplitude of the first pulse for IRMPD (for angiotensin I) and ECD (for substance P). The variation occurring at approximately 140  $V_{pp}$  in the curve corresponding to ECD is caused by a reloading of the sample. (b) Relative intensity of fragment ions  $c_4^+$  and  $c_5^+$  of substance P vs excitation amplitude of the first pulse for IR-ECD. (c) Relative intensity of fragment ions  $c_4$  and  $c_5$  of substance P vs excitation amplitude of the first pulse for IR-ECD. Relative intensities are measured by dividing by the maximum intensity in order to plot all intensities on the same scale.

The curve obtained in Figure 1a for IRMPD of the  $MH_3^{3+}$  ion of angiotensin I is very similar to the mapping of the IRMPD fragmentation zone of  $MH^+$  of triolein on a 9.4 T ApexQE instrument published in a previous article.<sup>14</sup> At the center of the ICR cell, the fragmentation efficiency was about 98%. The two instruments on which these experiments have

been conducted have very similar setups, both using Infinity ICR cells and identical  $CO_2$  lasers for IRMPD.<sup>30,35,36</sup>

Figure 1a also shows the fragmentation zone for ECD, using  $MH_2^{2+}$  of substance P as a precursor. Unlike the IRMPD fragmentation zone, in which the maximum fragmentation efficiency is obtained at the center of the ICR cell, the ECD fragmentation zone produces a maximum fragmentation efficiency of ~80% at approximately 70  $V_{pp}$  excitation. The ECD fragmentation zone appears to be around twice as large as the IRMPD fragmentation zone. This result is consistent with the experimental setup, in which the laser beam is focused on the center of the ICR cell and passes through the hollow cathode dispenser.<sup>30</sup> The disparity between the IRMPD and the ECD fragmentation zones means that the IR-ECD fragmentation zone is not easily mapped. Because IR irradiation activates peptide ions,  $c/z^+$  ion pairs separate readily after formation instead of during the delay between activation and excitation.<sup>25,37</sup> As a result,  $H^+$  cannot migrate in order to form  $c^+/z^+$  ion pairs. Therefore, for substance P,  $c_4^+$  and  $c_5^+$  are specific to ECD, since they are not present in IR-ECD MS/MS spectra, and they are present in ECD MS/MS spectra.<sup>26,27</sup> Figure 1b shows the relative intensity of  $c_4^+$  and  $c_5^+$  of substance P as a function of the RF excitation amplitude for the pulse sequence shown in Scheme 1a with IR-ECD fragmentation. For comparison, Figure 1c shows the relative abundance of  $c_4$  and  $c_5$ , which are present both in ECD and IR-ECD mass spectra, from the same experiment. Figure 1b shows that  $c_4^+$  and  $c_5^+$  are absent for amplitudes below 80  $V_{pp}$ , which corresponds well with the radius limit of the fragmentation zone for IRMPD. The abundances of  $c_4^+$  and  $c_5^+$  increase until 150  $V_{pp}$  before decreasing and disappearing again beyond 150  $V_{pp}$ , which corresponds to the edge of the ECD fragmentation zone. Therefore, the fragmentation zone for IR-ECD is ring-shaped for fragments that are only generated by ECD.

The shape of the fragmentation zone is different for each fragment ion of a given precursor, because each fragment is the result of a different fragmentation mechanism. Furthermore, the intensity of each fragment ion signal is a function of  $t_1$ . This function depends on the amplitude of the radius modulation of the precursor ion. For IR-ECD, the fragmentation zone is shaped by the laser beam profile and the electron beam profile in the ICR cell. Peptide fragments have different fragmentation zones according to the mechanisms that generate them. Peptide  $b/y$  fragments are generated by IRMPD fragmentation, which happens at the center of the ICR cell (excitation voltage less than 100  $V_{pp}$  in Figure 1a). Peptide  $c/z^+$  fragments are generated by the electron beam regardless of IR irradiation and have a much larger fragmentation zone (excitation voltage less than 230  $V_{pp}$  in Figure 1a). Peptide  $c^+$  fragments are generated by the electron beam only when IR irradiation is insufficient and have a ring-shaped fragmentation zone (excitation voltage between 100 and 230  $V_{pp}$  in Figure 1a).

Therefore,  $b/y$ ,  $c/z^+$ , and  $c^+$  fragments have different intensities as a function of  $t_1$  in 2D mass spectra. After Fourier transformation, vertical precursor ion scans are expected to show harmonic peaks with different relative intensities according to the type of fragment. In this study, the amplitude of  $P_1$  and  $P_2$  in the pulse sequence for 2D IR-ECD MS experiments (see Scheme 1b) is 180  $V_{pp}$ . For fragments that are generated by IR only ( $b/y$  fragments), the maximum radius of the modulation of precursor ions is twice the radius of the fragmentation zone. A previous study has shown that this leads to a high intensity of high order harmonics compared to the

intensity of the first harmonic in the precursor ion scan.<sup>14</sup> For fragments generated by the electron beam regardless of IR irradiation ( $c/z^{\bullet}$  fragments), the maximum radius of the modulation of precursor ions is almost the size of the fragmentation zone. According to the same study, this leads to low intensities of high order harmonics in the precursor ion scans compared to the intensity of the first order harmonic.<sup>14</sup> For fragment ions generated by the electron beam only if the IR irradiation is insufficient ( $c^{\bullet}$  fragments), the fact that the fragmentation zone is ring-shaped means that high order harmonics in the precursor ion scans can be predicted to have higher intensities than the first harmonic.

Figure 2a shows the 2D IR-ECD mass spectrum of substance P. The precursor ion  $m/z$  ratios are plotted vertically, and the

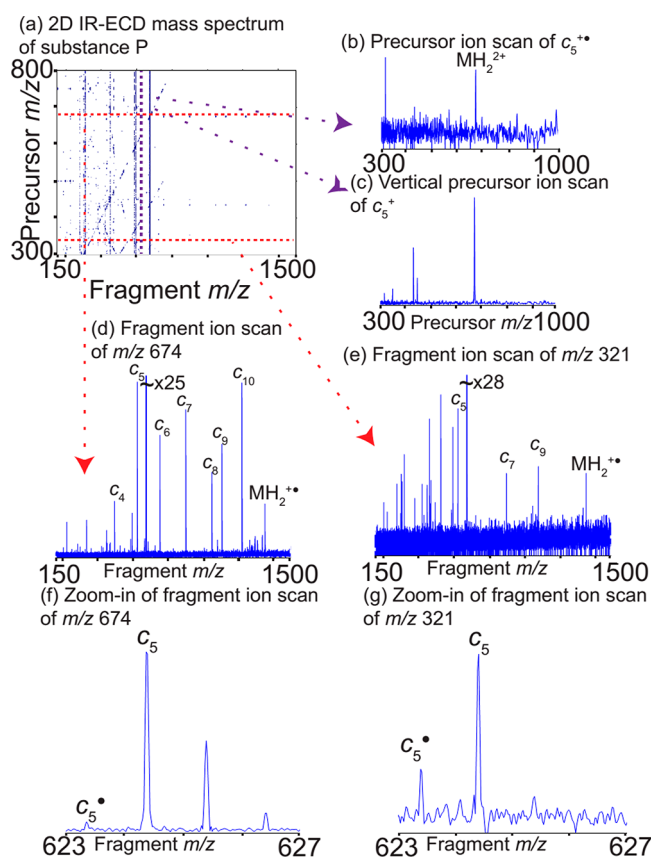


**Figure 2.** (a) 2D IR-ECD mass spectrum of substance P without denoising. (b) Vertical precursor ion scan of  $m/z$  623.39, corresponding to  $c_5^{\bullet}$ . (c) Vertical precursor ion scan of  $m/z$  624.39, corresponding to  $c_5$ . (d) Fragment ion scan of  $m/z$  674, corresponding to  $MH_2^{2+}$  of substance P. (e) Fragment ion scan of  $m/z$  321, corresponding to a harmonic of the signal from  $MH_2^{2+}$  of substance P. (f) Zoom-in from the fragment ion scan shown in (d) between  $m/z$  623–627, showing  $c_5^{\bullet}/c_5$ . (g) Zoom-in from the fragment ion scan shown in (e) between  $m/z$  623–627, showing  $c_5^{\bullet}/c_5$ .

fragment ion  $m/z$  ratios are plotted horizontally. Because the number of data points in the vertical precursor ion dimension is 2048 compared to 131 072 in the horizontal fragment ion dimension, the mass accuracy of precursor ion  $m/z$  ratios are 2 orders of magnitude smaller. Precursor ion  $m/z$  ratios are therefore reported with a 1 Da/e precision, and fragment ion  $m/z$  ratios are reported with a 0.01 Da/e precision. Figure 2b shows the precursor ion scan extracted from the 2D mass spectrum for  $m/z$  623.39 (corresponding to the  $c_5^{\bullet}$  fragment of

substance P), and Figure 2c shows the precursor ion scan for  $m/z$  624.39 (corresponding to the  $c_5$  fragment of substance P). The precursor ion scans both show a peak at  $m/z$  674, corresponding to  $MH_2^{2+}$  of substance P, showing the fragments resulting from the  $MH_2^{2+}$  ion. The precursor peak at  $m/z$  674 is small for  $c_5^{\bullet}$  but intense for  $c_5$ .

The precursor ion scans show other peaks corresponding to aliased harmonics of the signal. In the vertical dimension, the behavior of harmonics is different from the horizontal dimension, in which harmonics are present in the mass spectrum simply as peaks at fractions of the measured  $m/z$  ratio.<sup>38</sup> Bruker FTICR mass spectrometers use a phase accumulator at the lowest frequency of the waveform. In the present experiment, the lowest frequency in the excitation is 122.8 kHz, corresponding to  $m/z$  1500. As a result, all frequencies in the vertical dimension of the 2D mass spectrum are offset by 122.8 kHz, and harmonics and folded harmonics are offset by multiples of 122.8 kHz (i.e.,  $m/z$  1500).<sup>14</sup>

The precursor ion scans shown in Figure 2b,c both show a harmonic peak at  $m/z$  321. In the precursor ion scan of  $c_5^{\bullet}$ , the peaks at  $m/z$  674 and  $m/z$  321 have similar intensities. In the precursor ion scan of  $c_5$ , the peak at  $m/z$  321 has a much smaller intensity than the peak at  $m/z$  674. The  $c_5^{\bullet}$  fragment is specific to ECD, (see Figure 1b), whereas the  $c_5$  fragment is produced both by ECD and IR-ECD (see Figure 1c). The fragmentation zones of the two fragments are therefore different, and the signal intensities as functions of  $t_1$  are reflections of the fragmentation zones. The pulse sequence for 2D IR-ECD MS (see Scheme 1b) has been optimized for fragments that are produced both in ECD and IR-ECD.<sup>14</sup> The peaks corresponding to high order harmonics in the vertical precursor ion scan of  $c_5$  therefore have lower intensities than the first harmonic at  $m/z$  674. The pulse sequence is not optimized for the fragmentation zone of  $c_5^{\bullet}$ , and therefore, its vertical precursor ion scan has high order harmonic peaks that have a high intensity compared to the first harmonic at  $m/z$  674.

Comparison between the two signals may enable the distinction between the ECD and IR-ECD fragmentation patterns of substance P within the same 2D mass spectrum. In the raw 2D spectra, each horizontal fragment scan line is indicated by an integer (the index) between 1 and the number of data points in the vertical dimension (here, 2048). Each line (index) is correlated with frequency and thus  $m/z$  of the precursor fragmented. The fragment ion scan at  $m/z$  674 has a modulation frequency of 273.2 kHz and an index of 616. The fragment ion scan at  $m/z$  321 has a modulation frequency of 574.2 kHz and an index of 1848 ( $616 \times 3$ ). Therefore, the fragment ion scan at  $m/z$  321 corresponds to the third harmonic of the signal at  $m/z$  674, the  $MH_2^{2+}$  ion of substance P and its fragments, aliased twice by the vertical frequency offset. The correspondences between  $m/z$  ratio, frequency, and index in the vertical precursor ion dimension are recorded in Table S3 in the Supporting Information.

Figure 2d,e shows the extracted horizontal fragment ion scans at  $m/z$  674 and  $m/z$  321 respectively. The fragment ion scan at  $m/z$  674 shows the familiar fragmentation pattern of substance P.<sup>39</sup> The harmonic scan at  $m/z$  321 (Figure 2e) shows the same fragmentation pattern, but with a lower signal-to-noise ratio than Figure 2d, as expected. Figure 2f shows a zoom-in between  $m/z$  623–627 for the fragment ion scan of  $m/z$  674. The peak corresponding to  $c_5^{\bullet}$  has a relative abundance of 6% compared with the peak corresponding to  $c_5$ , which is characteristic of the IR-ECD fragmentation of

substance P.<sup>27</sup> Figure 2g shows a zoom-in between  $m/z$  623–627 for the fragment ion scan of  $m/z$  321. The peak corresponding to  $c_5^+$  has a relative abundance of 36% compared to the peak corresponding to  $c_5$ , which is characteristic of the ECD fragmentation of substance P.<sup>27</sup> This result stems from the fact that the fragmentation zone for ECD-only fragments is different from the fragmentation zone for fragments produced in ECD and IR-ECD (see Figure 2b,c). The comparison between fragment ion scans and their harmonics in the 2D mass spectrum therefore opens up the possibility to distinguish between ECD and IR-ECD fragmentation patterns in a single experiment.

### 2D IR-ECD Mass Spectrum of the Tryptic Digest of Cytochrome c. Figure 3 shows the 2D IR-ECD mass

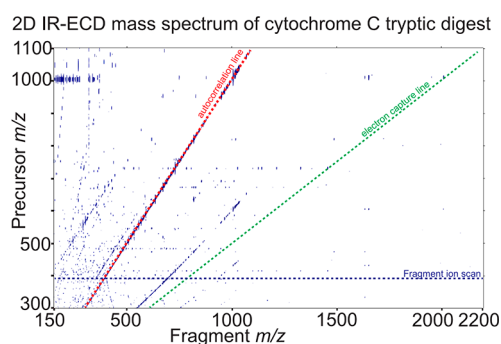


**Figure 3.** 2D IR-ECD mass spectrum of the cytochrome c tryptic digest.

spectrum of the tryptic digest of cytochrome c. The two first pulses in the 2D MS experimental script are set at 180 V<sub>pp</sub>. The autocorrelation line (shown in red) contains the peaks for the precursor ions whose abundances and radii are modulated according to their own cyclotron frequency. The electron capture line shown in green shows the peaks corresponding to the charge-reduced radical cation species from doubly charged peptides.<sup>21</sup> The autocorrelation line has a slope of 1, and the electron capture line has a slope of 1/2 for doubly charged peptides. The horizontal fragment ion scan of MH<sub>2</sub><sup>2+</sup> of TGP<sup>+</sup>NLHGLFGR at  $m/z$  584.9 was internally calibrated using a quadratic frequency-to-mass conversion equation.<sup>33</sup> This calibration equation was then applied to all horizontal fragment ion scans in the 2D mass spectrum. The autocorrelation line and the electron capture line were extracted and are shown in Figure S3 in the Supporting Information. The resolving power at  $m/z$  400 is 100 000 in the horizontal fragment ion dimension and 800 in the vertical precursor ion dimension.

All assigned peaks are listed in the Supporting Information (Table S5). The cleavage coverage obtained is shown in Scheme S1 of the Supporting Information: the cleavage coverage was 41/103 residues. The IR irradiation length was optimized to activate doubly charged peptides containing about 10 residues. However, the IR irradiation proved to be sufficient to fragment smaller peptides or triply charged peptides. As a result, the 2D IR-ECD experiment lead to some  $b/y$  fragmentations in addition to  $c/z$  fragmentations caused by ECD, and certain cleavages were redundant.

Figure S1 in the Supporting Information shows the 2D ECD mass spectrum of the tryptic digest of cytochrome c. The two 2D mass spectra were acquired in identical conditions, except for the fact that in the 2D IR-ECD mass spectrum, ECD irradiation was preceded by IR irradiation. All assigned peaks

are listed in the Supporting Information (Table S6). The cleavage coverage obtained is shown in Scheme S2: the cleavage coverage was 40/103 residues. Because there was no IR irradiation, very few  $b/y$  fragmentations were observed in addition to  $c/z$  fragmentations, which lead to very little cleavage redundancy.

Figure 4 shows two extracted fragment ion scans from the 2D IR-ECD mass spectrum. Figure 4a shows the extracted

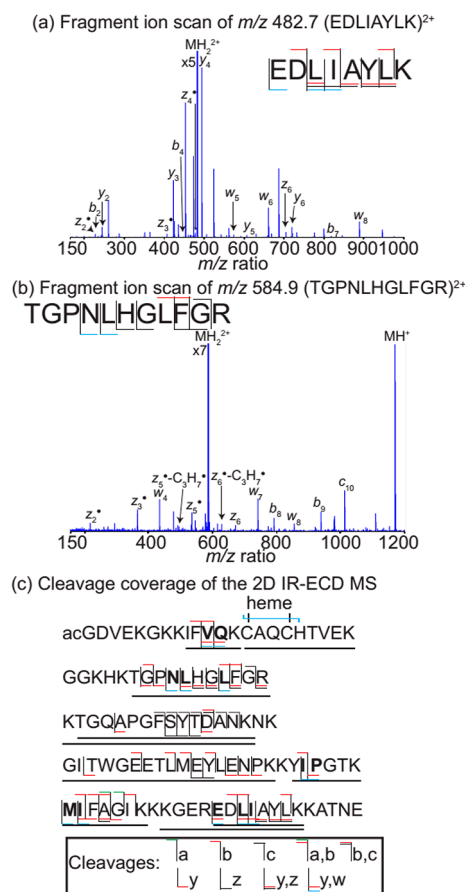


**Figure 4.** (a) Fragment ion scan of  $m/z$  482.7 extracted from the 2D IR-ECD mass spectrum of the tryptic digest of cytochrome c. (b) Fragment ion scan of  $m/z$  584.9 extracted from the 2D IR-ECD mass spectrum of the tryptic digest of cytochrome c. (c) Cleavage coverage of cytochrome c obtained in the 2D IR-ECD mass spectrum. Residues cleaving into  $w$  ions in bold lettering.

fragment ion scan for  $m/z$  482.7, which corresponds to the EDLIAYLK<sup>2+</sup> peptide. The fragmentation pattern consists of both  $y$  and  $z$  fragments on the C-terminus and  $b$  fragment ions the N-terminus. The fragmentation pattern observed (see Supporting Information, Table S5) was very similar to the fragmentation pattern obtained in the 2D ECD mass spectrum of the tryptic digest of cytochrome c (see Supporting Information, Table S6). In total, six out of seven residues were cleaved. In addition, three  $w$  fragment ions were identified:  $w_5$ ,  $w_6$ , and  $w_8$  (also called  $w_a$  fragments). These fragment ions correspond to side-chain losses that are characteristic of IR-ECD<sup>25</sup> and characteristic to each residue. Their presence in the fragment ion scan allows the differentiation of leucine and isoleucine residues.<sup>40–43</sup> The EDLIAYLK<sup>2+</sup> precursor ion contains three leucine/isoleucine

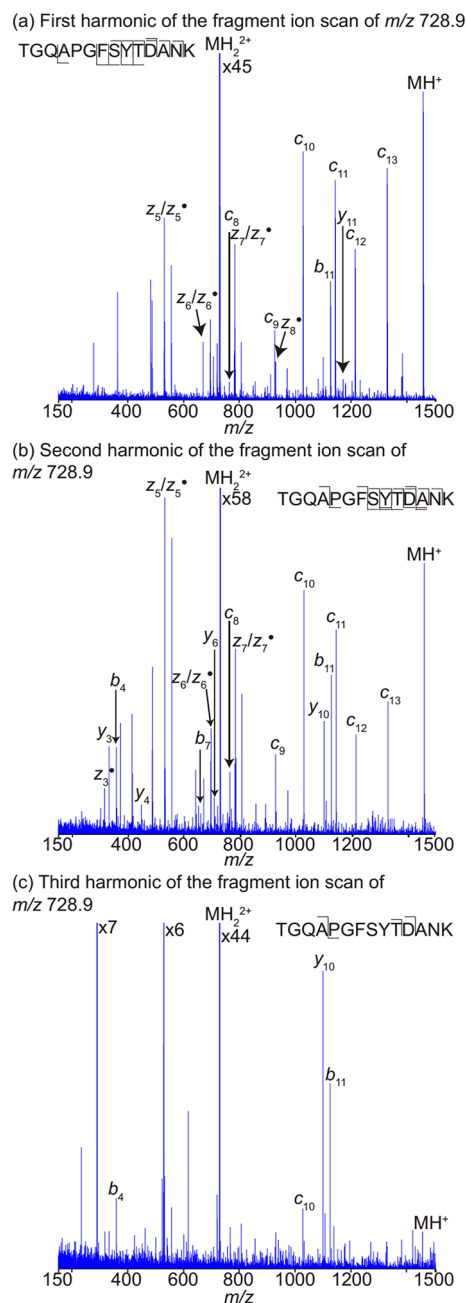
residues. The presence of  $w$  fragment ions enables the unambiguous identification of the  $L_3$  and  $L_4$  residues.

Figure 4b shows the extracted fragment ion scan at  $m/z$  584.9, which corresponds to TGPLNHGLFGR<sup>2+</sup>. The fragmentation pattern shows mainly  $c/z$  fragments. In this fragment ion scan, 5 out of 10 residues are cleaved (see Supporting Information, Table S5). This peptide is also ionized as a triply charged ion species. The fragmentation pattern of TGPLNHGLFGR<sup>2+</sup> combined with the fragmentation pattern of TGPLNHGLFGR<sup>3+</sup> shows that 8 out of 10 residues are cleaved (see Scheme S1). The simultaneous fragmentation of compounds with different charge states is one of the ways that two-dimensional mass spectrometry leads to enhanced sequence information.<sup>18,20–22</sup> The fragmentation of TGPLNHGLFGR<sup>2+</sup>, like the fragmentation of EDLIAYLK<sup>2+</sup>, leads to side-chain losses:  $w_4$ ,  $w_7$ , and  $w_8$ . Fragment  $w_8$  corresponds to a side-chain loss from asparagine, whereas the  $w_4$  and  $w_7$  fragments correspond to a side-chain loss from leucine. The presence of these two fragments in the fragment ion scan enables the unambiguous identification of the two leucine residues. The loss of  $C_3H_7^{\bullet}$  from two  $z^{\bullet}$  fragments is also indicative of the presence of leucine residues in the peptide, which assists with peptide sequencing in the case of an unknown peptide.<sup>44,45</sup>

All the residues in cytochrome *c* that fragment with side-chain losses in the 2D IR-ECD mass spectrum are shown in bold in Figure 4c. The cytochrome *c* protein contains 12 leucine or isoleucine residues: 6 of them can be conclusively identified with the  $w$  fragments observed herein.

Figure 5 shows the fragment ion scan of  $m/z$  728.9 corresponding to the fragmentation of TGQAPGFSYTDANK<sup>2+</sup> (Figure 5a), the harmonic extracted at twice the index of the fragment ion scan at  $m/z$  728.9 (second harmonic minus the cyclotron frequency at the maximum  $m/z$  ratio, shown in Figure 5b), and the harmonic sampled at three times the index of the fragment ion scan at  $m/z$  728.9 (third harmonic minus twice the cyclotron frequency at the maximum  $m/z$  ratio, shown Figure 5c). The correspondences between  $m/z$  ratio, frequency, and index in the vertical precursor ion dimension are recorded in Table S4 in the Supporting Information. The fragment ion scan in Figure 5a shows a fragmentation pattern consisting of mostly  $c$  and  $z^{\bullet}$  ions, as expected. The second harmonic in Figure 5b shows that several  $b$  and  $y$  fragments appear. In the third harmonic shown in Figure 5c, only  $b_4$ ,  $b_{11}$ ,  $y_{10}$ , and  $c_{10}$  at low abundance remain in the extracted line. The harmonics show an increase in  $b/y$  ions compared to  $c/z$  ions. This phenomenon is very noticeable with the  $b_{11}/c_{11}$  peaks: in the fragment ion scan (Figure 5a), the relative intensity of  $b_{11}/c_{11}$  is 55%; in the second harmonic (Figure 5b), the relative intensity of  $b_{11}/c_{11}$  is 80%; and in the third harmonic (Figure 5c),  $c_{11}$  is not present anymore. Conversely, for the  $z_6^{\bullet}/y_6$  peaks,  $y_6$  is not present in the fragment ion scan (Figure 5a) but has an intensity of 30% compared to  $z_6^{\bullet}$  in the second harmonic (Figure 5a). Figure S4 in the Supporting Information shows the harmonics of the fragment ion scans at  $m/z$  482.9, corresponding to  $MH_2^{2+}$  of peptide EDLIAYLK, which shows similar behavior for three fragment ion pairs:  $z_3^{\bullet}/y_3$ ,  $z_4^{\bullet}/y_4$ , and  $z_6^{\bullet}/y_6$ .

The difference in behavior between  $c/z$  ions and  $b/y$  ions can be explained by the difference in the shape and size of the fragmentation zones for IR and ECD fragmentation. As shown in Figure 1a, the IR fragmentation zone is smaller than the ECD fragmentation zone. As a result, the amplitude of the



**Figure 5.** (a) Fragment ion scan of  $m/z$  728.9 extracted from the 2D IR-ECD mass spectrum of cytochrome *c* tryptic digest. (b) Second harmonic of the fragment ion scan of  $m/z$  728.9. (c) Third harmonic of the fragment ion scan of  $m/z$  728.9. The peaks labeled  $\times 6$  and  $\times 7$  correspond to internal fragments that are cut off at 1/6th and 1/7th of their intensity, respectively.

precursor ion radius is much larger than the fragmentation zone for  $b/y$  fragment ions. A previous study has shown that when the amplitude of the precursor ion radius goes far outside of the fragmentation zone; the harmonics in the vertical precursor ion dimension are intense.<sup>14</sup> The amplitude of the encoding pulses in the pulse sequence (see Scheme 1b) is 180 V<sub>pp</sub>, which means that the maximum ion radius at the end of the encoding sequence covers the ECD fragmentation zone but goes far outside of the IR irradiation zone (see Figure 1a). Because the parameters of the encoding pulses modulating the precursor ion radii (see Scheme 1b) were optimized for ECD

fragmentation,  $c/z$  fragment ions are not very intense in the second and third harmonic of the fragment ion scan. However, because the modulation goes far outside of the IR fragmentation zone,  $b/y$  fragments are intense in the second and third harmonic of the fragment ion scan.

This property of 2D IR-ECD mass spectrometry can be used in order to differentiate between N-terminal and C-terminal fragments. If two fragments are separated by a mass of 15.010899 Da (NH) or 14.003074 Da (N), then the evolution of their intensity at higher harmonics gives an indication as to whether they are N-terminal or C-terminal. For fragment couples in which the ion at lower  $m/z$  ratio has an intensity that increases compared to the ion at higher  $m/z$  ratio, then the two peaks are  $b/c^\bullet$  or  $b/c$  ions. For fragment couples in which the ion at lower  $m/z$  ratio has an intensity that decreases compared to the ion at higher  $m/z$  ratio, then the two peaks are  $y/z^\bullet$  or  $y/z$  ions.<sup>26,27</sup>

In the 2D IR-ECD mass spectrum of unknown peptides, an algorithm can easily be developed by peak-picking the fragment ion scan of a given peptide and its harmonics. Peak pairs with mass differences of 15.010899 or 14.003074 Da can be identified. The progression with increasing harmonic order of the ratio between intensities of the peak pairs can be calculated to distinguish a  $b/c$  peak pair from a  $z/y$  peak pair in order to assign the N-terminus and the C-terminus of the peptide. Only one peak pair is needed per peptide in order to make this assignment.

Peak assignments for the second and third harmonic of fragment ions are shown in Tables S7 and S8 of the Supporting Information. Most of the fragments in the harmonics are  $b/y$  ions and  $w$  ions, which were probably also generated in the IR fragmentation zone and therefore had the same behavior as  $b/y$  ions in terms of vertical harmonics. All the fragments from the fragment ion scans; the second harmonic and third harmonic are shown in Scheme S3 in the Supporting Information. The harmonic lines produce a few more cleavages than the fragment ion scans alone: altogether 48/103 residues are cleaved. Figure 6a shows the region containing the  $z_6$  fragment ion of GITWGEETLMEYLENPK<sup>2+</sup>. The autocorrelation line shows that this peptide is also oxidized at the methionine (see Figure S3 in the Supporting Information). The nonmodified peptide and the oxidized peptide both have a fragment at the same  $m/z$  ratio that are vertical to one another in the 2D mass spectrum. As a result, the fragment can be identified as the  $z_6$  fragment of the oxidized peptide, and the oxidation can be located between residue 1 and 11 of the peptide.

Figure 6b shows the region of the  $b_{14}^{2+}$  fragment of GITWGEETLMEYLENPK<sup>3+</sup>. A fragment of the oxidized form of GITWGEETLMEYLENPK<sup>3+</sup> is on the same dissociation line as the isotopic distribution of  $b_{14}^{2+}$  of the nonmodified peptide. In the present dissociation, the slope of the dissociation line is predicted to be 2/3, because the precursor is triply charged, and the fragment is doubly charged. The intercept is predicted to be  $357.2007/3 = 119.0669$  (the mass of the complementary  $y_3$  fragment, i.e., NPK, is 357.2007 Da). As a result, the fragment can be identified as the  $b_{14}^{2+}$  fragment of the oxidized peptide, and the oxidation can be located between residue 1 and 14 of the peptide. Because 2D mass spectrometry is a data-independent acquisition technique, the fragmentation pattern of both the unmodified and the oxidized peptide are recorded in the 2D mass spectrum. A visual comparison between the fragmentation patterns in the

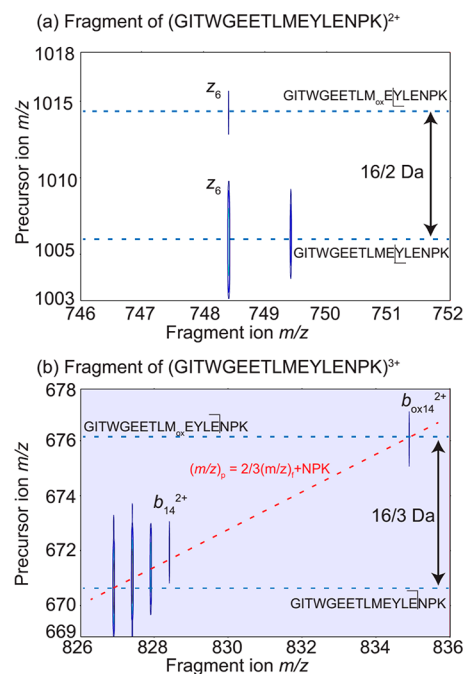


**Figure 6.** (a) Zoom-in on the region containing the  $z_6$  fragment ion of (GITWGEETLMEYLENPK)<sup>2+</sup> from the 2D IR-ECD mass spectrum of the tryptic digest of cytochrome c. (b) Zoom-in on the region containing the  $b_{14}^{2+}$  fragment ion of (GITWGEETLMEYLENPK)<sup>3+</sup> from the 2D IR-ECD mass spectrum of the tryptic digest of cytochrome c. In the equation of the dissociation line,  $(m/z)_p$  corresponds to the  $m/z$  ratio of the precursor ion, and  $(m/z)_f$  corresponds to the  $m/z$  ratio of the fragment ion.

2D mass spectrum gives indications as to the location of the modification.

## CONCLUSION

In this study, two-dimensional IR-ECD mass spectrometry was implemented and optimized. The difference in the size and shape of the fragmentation zones for IR irradiation and ECD irradiation lead to different abundance modulations for IR-induced fragments, ECD-induced fragments, and IR-ECD-induced fragments, and therefore to different relative abundances in their vertical harmonics.

2D IR-ECD mass spectrometry was shown to have the advantage of combining the two fragmentation methods by producing both  $c/z$  fragments and  $b/y$  fragments, which improved cleavage coverage on tryptic peptides from cytochrome c, especially when the fragmentation patterns from the high order harmonics are included. In addition, IR-ECD caused increased residue side-chain losses that lead to the distinction between leucine and isoleucine residues, which are isomeric.

Extracting vertical harmonic lines showed that  $b/y$  fragments induced by IR irradiation have a different abundance modulation than  $c/z$  fragments and that their relative abundance tends to increase in vertical harmonics. This property enabled the distinction between N-terminal and C-terminal fragments in a single experiment for all peptides in a complex sample.

Finally, this study showed that peptide modifications can be identified and located by using the relative positions of fragments from the modified and the nonmodified peptide. This property is not only useful for peptide sequencing but also

for the identification and location of post-translational modifications in top-down proteomics.<sup>22,46</sup>

This study has shown that 2D IR-ECD mass spectrometry is a powerful analytical tool for peptide sequencing in complex samples and that it brings information that standard MS/MS does not. This study also shows that the vertical harmonics in 2D mass spectra contain important and useful analytical information. As a result, the abundance modulation of fragments and their relative abundances in vertical harmonics can be said to deserve more in-depth study.

## ■ ASSOCIATED CONTENT

### ■ Supporting Information

The Supporting Information is available free of charge on the ACS Publications website at DOI: 10.1021/acs.analchem.7b05324.

Principle of 2D mass spectrometry. Instrument parameters for MS/MS spectra. Instrument parameters for 2D mass spectra. List of fragments identified in the 2D mass spectrum using IR-ECD as a fragmentation mode (first harmonic). Cleavage coverage of cytochrome c obtained in the 2D IR-ECD mass spectrum. 2D ECD mass spectrum of the cytochrome c tryptic digest. List of fragments identified in the 2D mass spectrum using ECD as a fragmentation mode. Cleavage coverage of cytochrome c obtained in the 2D ECD mass spectrum. List of fragments identified in the 2D mass spectrum using IR-ECD as a fragmentation mode (second harmonic). List of fragments identified in the 2D mass spectrum using IR-ECD as a fragmentation mode (third harmonic). Cleavage coverage of cytochrome c obtained in the 2D IR-ECD mass spectrum including fragmentation patterns obtained from the second and third harmonics of extracted fragment ion scans. Example of data processing program for the fragmentation zone mapping. Autocorrelation line and electron capture line (doubly charged ions capturing one electron) extracted from the 2D IR-ECD mass spectrum of the cytochrome c tryptic digest. Fragment ion scan of  $m/z$  482.7 extracted from the 2D IR-ECD mass spectrum of cytochrome c tryptic digest, second harmonic of the fragment ion scan of  $m/z$  482.7, and third harmonic of the fragment ion scan of  $m/z$  482.7 (PDF)

## ■ AUTHOR INFORMATION

### Corresponding Author

\*E-mail: p.oconnor@warwick.ac.uk; Telephone: +44 (0)2476 151008 (P.B.O)

### ORCID

Mark P. Barrow: 0000-0002-6474-5357

### Author Contributions

The manuscript was written through contributions of all authors. All authors have given approval to the final version of the manuscript.

### Funding

The authors would like to thank the Warwick Impact Fund Proof-of-Concept Award and the EPSRC Impact Acceleration Award, the Engineering and Physical Sciences Research Council for grant number EP/J000302/1 and grant number EP/N021630/1, the Biotechnology and Biological Sciences

Research Council for grant number BB/P021875/1, and the Royal Society Translation Award.

### Notes

The authors declare no competing financial interest.

## ■ ACKNOWLEDGMENTS

The authors would like to thank Dr. Christian Rolando for helpful conversations and the Centre for Scientific Computing at the University of Warwick for the use of their server for data processing. The authors would also like to thank the Warwick Impact Fund Proof-of-Concept Award and the EPSRC Impact Acceleration Award, the Engineering and Physical Sciences Research Council for grant number EP/J000302/1 and grant number EP/N021630/1, the Biotechnology and Biological Sciences Research Council for grant number BB/P021875/1, and the Royal Society Translation Award for funding this research.

## ■ REFERENCES

- (1) van Agthoven, M. A.; Delsuc, M.-A.; Bodenhausen, G.; Rolando, C. *Anal. Bioanal. Chem.* **2013**, *405*, 51–61.
- (2) Comisarow, M. B.; Marshall, A. G. *Chem. Phys. Lett.* **1974**, *25*, 282–283.
- (3) Pfändler, P.; Bodenhausen, G.; Rapin, J.; Houriet, R.; Gäumann, T. *Chem. Phys. Lett.* **1987**, *138*, 195–200.
- (4) Pfändler, P.; Bodenhausen, G.; Rapin, J.; Walser, M. E.; Gäumann, T. *J. Am. Chem. Soc.* **1988**, *110*, 5625–5628.
- (5) Bensimon, M.; Zhao, G.; Gäumann, T. *Chem. Phys. Lett.* **1989**, *157*, 97–100.
- (6) Marshall, A. G.; Lin Wang, T. C.; Lebatuan Ricca, T. L. *Chem. Phys. Lett.* **1984**, *105*, 233–236.
- (7) Guan, S.; Jones, P. R. *J. Chem. Phys.* **1989**, *91*, 5291–5295.
- (8) Williams, E. R.; Loh, S. Y.; McLafferty, F. W.; Cody, R. B. *Anal. Chem.* **1990**, *62*, 698–703.
- (9) Ross, C. W., III; Guan, S.; Grosshans, P. B.; Ricca, T. L.; Marshall, A. G. *J. Am. Chem. Soc.* **1993**, *115*, 7854–7861.
- (10) Ross, C. W.; Simonsick, W. J.; Aaserud, D. J. *Anal. Chem.* **2002**, *74*, 4625–4633.
- (11) van der Rest, G.; Marshall, A. G. *Int. J. Mass Spectrom.* **2001**, *210–211*, 101–111.
- (12) van Agthoven, M. A.; Delsuc, M.-A.; Rolando, C. *Int. J. Mass Spectrom.* **2011**, *306*, 196–203.
- (13) van Agthoven, M. A.; Chiron, L.; Coutouly, M.-A.; Delsuc, M.-A.; Rolando, C. *Anal. Chem.* **2012**, *84*, 5589–5595.
- (14) van Agthoven, M. A.; Chiron, L.; Coutouly, M.-A.; Sehgal, A. A.; Pelupessy, P.; Delsuc, M.-A.; Rolando, C. *Int. J. Mass Spectrom.* **2014**, *370*, 114–124.
- (15) van Agthoven, M. A.; Coutouly, M.-A.; Rolando, C.; Delsuc, M.-A. *Rapid Commun. Mass Spectrom.* **2011**, *25*, 1609–1616.
- (16) Chiron, L.; van Agthoven, M. A.; Kieffer, B.; Rolando, C.; Delsuc, M.-A. *Proc. Natl. Acad. Sci. U. S. A.* **2014**, *111*, 1385–1390.
- (17) Chiron, L.; Coutouly, M.-A.; Starck, J.-P.; Rolando, C.; Delsuc, M.-A. SPIKE: A Processing Software dedicated to Fourier Spectroscopies. **2016**, arXiv:1608.06777. arXiv.org e-Print Archive.
- (18) van Agthoven, M. A.; Barrow, M. P.; Chiron, L.; Coutouly, M.-A.; Kilgour, D.; Wootton, C. A.; Wei, J.; Soulby, A.; Delsuc, M.-A.; Rolando, C.; O'Connor, P. B. *J. Am. Soc. Mass Spectrom.* **2015**, *26*, 2105–2114.
- (19) Floris, F.; Vallotto, C.; Chiron, L.; Lynch, A. M.; Barrow, M. P.; Delsuc, M.-A.; O'Connor, P. B. *Anal. Chem.* **2017**, *89*, 9892–9899.
- (20) Simon, H. J.; van Agthoven, M. A.; Lam, P. Y.; Floris, F.; Chiron, L.; Delsuc, M. A.; Rolando, C.; Barrow, M. P.; O'Connor, P. B. *Analyst* **2016**, *141*, 157–165.
- (21) van Agthoven, M. A.; Wootton, C. A.; Chiron, L.; Coutouly, M.-A.; Soulby, A.; Wei, J.; Barrow, M. P.; Delsuc, M.-A.; Rolando, C.; O'Connor, P. B. *Anal. Chem.* **2016**, *88*, 4409–4417.

- (22) Floris, F.; van Agthoven, M.; Chiron, L.; Soulby, A. J.; Wootton, C. A.; Lam, Y. P. Y.; Barrow, M. P.; Delsuc, M.-A.; O'Connor, P. B. *J. Am. Soc. Mass Spectrom.* **2016**, *27*, 1531–1538.
- (23) van Agthoven, M. A.; O'Connor, P. B. *Rapid Commun. Mass Spectrom.* **2017**, *31*, 674–684.
- (24) Bray, F.; Bouclon, J.; Chiron, L.; Witt, M.; Delsuc, M.-A.; Rolando, C. *Anal. Chem.* **2017**, *89*, 8589–8593.
- (25) Lin, C.; Cournoyer, J. J.; O'Connor, P. B. *J. Am. Soc. Mass Spectrom.* **2008**, *19*, 780–789.
- (26) Horn, D. M.; Ge, Y.; McLafferty, F. W. *Anal. Chem.* **2000**, *72*, 4778–4784.
- (27) Tsybin, Y. O.; He, H.; Emmett, M. R.; Hendrickson, C. L.; Marshall, A. G. *Anal. Chem.* **2007**, *79*, 7596–7602.
- (28) Dancik, V.; Addona, T. A.; Clauser, K. R.; Vath, J. E.; Pevzner, P. A. *J. Comput. Biol.* **1999**, *6*, 327–342.
- (29) Perkins, D. N.; Pappin, D. J. C.; Creasy, D. M.; Cottrell, J. S. *Electrophoresis* **1999**, *20*, 3551–3567.
- (30) Tsybin, Y. O.; Witt, M.; Baykut, G.; Kjeldsen, F.; Hakansson, P. *Rapid Commun. Mass Spectrom.* **2003**, *17*, 1759–1768.
- (31) Francl, T. J.; Sherman, M. G.; Hunter, R. L.; Locke, M. J.; Bowers, W. D.; McIver, R. T., Jr. *Int. J. Mass Spectrom. Ion Processes* **1983**, *54*, 189–199.
- (32) Shi, S. D. H.; Drader, J. J.; Freitas, M. A.; Hendrickson, C. L.; Marshall, A. G. *Int. J. Mass Spectrom.* **2000**, *195-196*, 591–598.
- (33) Ledford, E. B., Jr.; Rempel, D. L.; Gross, M. L. *Anal. Chem.* **1984**, *56*, 2744–2748.
- (34) Gorshkov, M. V.; Nikolaev, E. N. *Int. J. Mass Spectrom. Ion Processes* **1993**, *125*, 1–8.
- (35) Caravatti, P.; Allemann, M. *Org. Mass Spectrom.* **1991**, *26*, 514–518.
- (36) Little, D. P.; Speir, J. P.; Senko, M. W.; O'Connor, P. B.; McLafferty, F. W. *Anal. Chem.* **1994**, *66*, 2809–2815.
- (37) Leymarie, N.; Costello, C. E.; O'Connor, P. B. *J. Am. Chem. Soc.* **2003**, *125*, 8949–8958.
- (38) Schweihard, L.; Lindinger, M.; Kluge, H. J. *Int. J. Mass Spectrom. Ion Processes* **1990**, *98*, 25–33.
- (39) Zubarev, R. A.; Kelleher, N. L.; McLafferty, F. W. *J. Am. Chem. Soc.* **1998**, *120*, 3265–3266.
- (40) Savitski, M. M.; Nielsen, M. L.; Zubarev, R. A. *Anal. Chem.* **2007**, *79*, 2296–2302.
- (41) Johnson, R. S.; Martin, S. A.; Biemann, K.; Stults, J. T.; Watson, J. T. *Anal. Chem.* **1987**, *59*, 2621–2625.
- (42) Johnson, R. S.; Martin, S. A.; Biemann, K. *Int. J. Mass Spectrom. Ion Processes* **1988**, *86*, 137–154.
- (43) Alexander, A. J.; Boyd, R. K. *Int. J. Mass Spectrom. Ion Processes* **1989**, *90*, 211–240.
- (44) Cooper, H. J.; Hudgins, R. R.; Hakansson, K.; Marshall, A. G. *J. Am. Soc. Mass Spectrom.* **2002**, *13*, 241–249.
- (45) Fung, Y. M. E.; Chan, T. W. D. *J. Am. Soc. Mass Spectrom.* **2005**, *16*, 1523–1535.
- (46) Mann, M.; Jensen, O. N. *Nat. Biotechnol.* **2003**, *21*, 255–261.